Utility of respiratory-gated small-animal PET/CT in the chronologic evaluation of an orthotopic lung cancer transplantation mouse model

Tamaki Otani[1,6], Hideki Otsuka[2], Kazuya Kondo[3], Hiromitsu Takizawa[4], Motoi Nagata[1,6], Mina Kishida[5], Hirokazu Miyoshi[6]

1 Program in Medical Imaging Biosciences, Division of Health sciences, The University of Tokushima Graduate School, 3-18-15 Kuramoto-cho 3, Tokushima 770-8503, Japan

2 Department of Medical Imaging Biosciences, Institute of Health Biosciences, The University of Tokushima Graduate School, 3-18-15 Kuramoto-cho 3, Tokushima 770-8503, Japan

3 Department of Oncological Medical Services, Institute of Health Biosciences, The University of Tokushima Graduate School, 3-18-15 Kuramoto-cho 3, Tokushima 770-8503, Japan

4 Department of Thoracic, Endocrine and Oncological Surgery, Institute of Health Biosciences, The University of Tokushima Graduate School, 18-15 Kuramoto-cho 3, Tokushima 770-8503, Japan

5 Program in Radiological Technology, Division of Health Science, The University of Tokushima Graduate School, 3-18-15 Kuramoto-cho 3, Tokushima 770-8503, Japan

6 Radioisotope Research Center, The University of Tokushima Graduate School, 3-18-15

Kuramoto-cho 3, Tokushima 770-8503, Japan

corresponding author: Otani Tamaki

E-mail address: otani.tamaki@tokushima-u.ac.jp

Telephone number: +81-88-633-9207

Fax number: +81-88-633-9417

The type of article : Original article

Abstract

Our aim in this study was to clarify the effects of respiratory-gated PET in the evaluation of lung cancer according to the ^{18}F-FDG uptake in an orthotopic transplantation mouse model. We created such a model, and we performed PET/CT. The mice were divided into two groups according to tumor volume: a small-tumor group (<20 mm^3) and a large-tumor group (>20 mm^3). We reconstructed the following conditions based on list-mode data: non-gated (3D) images and gated (4D) images, divided based on the respiratory cycle (expiration phase, stable phase, and inspiration phase). We calculated the maximum standardized uptake values (SUV_{max}) in each phase. We used the % difference [= (4D SUV_{max} − 3D SUV_{max})/3D PET SUV_{max} × 100 (%)] to evaluate the differences in the 4D SUV_{max} and 3D SUV_{max}. The 4D SUV_{max} values were significantly higher than the 3D SUV_{max}, regardless of the tumor size. The % difference for the small tumors was greater than that for the large tumors, and it was highest in the stable phase. We conclude that the SUV_{max} in the stable phase under respiratory-gated PET are the most reliable. The SUV_{max} observed under non-gated PET are considered to be more frequently underestimated in cases involving small tumors than in those involving large tumors. In the chronologic study evaluating the time course of tumor development, the size of the tumor is small in early stage, and respiratory-gated PET is effective in reducing the underestimation of such tumors caused by respiratory motion.

Keywords

Respiratory-gated PET/CT • Small animals • Orthotopic lung cancer

Introduction

[^{18}F]-fluoro-2-deoxy-D-glucose (^{18}F-FDG) positron emission tomography/computed tomography (PET/CT) is an excellent method for imaging tumors and the most commonly used imaging modality for accurately delineating tumor lesions (1, 2). In recent years, the use of PET/CT equipment designed for small animals has spread widely, and this modality plays an important role at the forefront of clinical research (3, 4). In order to obtain an accurate quantification of radiotracer concentration, one must take several factors into account, such as attenuation (5), scatter (6), the partial volume effect (7), and motion.

We have been conducting a study to evaluate lung tumors in an orthotopic mouse model by using small-animal PET/CT (8). In this study, the target lesion was located in the lungs; therefore, we were concerned with the effects of respiratory movement. Respiratory movement and respiratory-gated PET have been discussed extensively in the literature on human PET studies (9-15). In human PET studies, respiratory motion causes a distortion in the morphology, i.e., poor shape definition. In addition, it induces a decrease in the counts from pulmonary lesions in the lungs, possibly limiting the sensitivity of lesion detection. The effects of respiratory movement vary with the lesion size; FDG uptake is underestimated in small-sized tumors (16).

In the chronologic study evaluating the time course of tumor development, the size of the tumor is small in early stage. Therefore, FDG uptake might be underestimated. Respiratory-gated PET imaging can be performed in small animals. Therefore, gating PET could be useful for correcting the effect of respiratory motion on tumor uptake in small animals. However, only a few reports have focused on respiratory PET for such animals (17). Moreover, the utility of respiratory-gated PET is controversial in animal studies. Our purpose in this study was to clarify the utility of respiratory PET in chronologically evaluated lung cancer according to ^{18}F-FDG uptake in an orthotopic transplantation mouse model.

Materials and methods

Animal model

Male SCID mice (CB-17/Icr-scidJc1, CLEA Japan Inc., Tokyo, Japan) at 6–8 weeks of age were used in this study and maintained in the Laboratory for Animal Experiments. The protocols for all animal experiments were approved by and carried out according to the guidelines of the Institutional Animal Care and Use Committee of the University of Tokushima, School of Medicine.

Cell lines

Two types of human non-small-cell lung cancer cell lines were used in this study (Ma44-3 [human squamous cell lung cancer] and A549 [human adenocarcinoma lung cancer]). The cell lines were cultured in RPMI 1640 (Sigma Chemical Co., St. Louis, MO, USA) with 10% heat inactivated fetal bovine serum (Bio Whittaker, Walkersville, MD, USA) and were maintained at 37°C in a humidified incubator with 5% CO_2 in air.

Orthotopic intrapulmonary implantation

For in our previous studies (18, 19), the mice were fully anesthetized via ether inhalation and placed in the left lateral decubitus position with the four limbs restrained. A 1-cm transverse incision was made in the right lateral skin just below the inferior border of the scapula in each SCID mouse. The muscles were separated from the ribs by sharp dissection, and the intercostal muscles were exposed. The right lung was made visible through the intercostal muscles. A 30-gauge needle was inserted approximately 5 mm into the lungs through the intercostal muscle, and an inoculum of 2×10^6 tumor

cells/mL with 400 mg/mL of Matrigel (Collaborative Biomedical Products, Bedford, Canada) was then dispersed into the right lung at a final volume of 10 mL (2×10^4 cells) of medium. The procedure required approximately 1 min for completion and was easily performed. The skin incision was closed with 3-0 silk. To validate *in vivo* FDG uptake, we performed orthotopic implantation in the right lung in order clearly to delineate tumor uptake from heart uptake (20, 21).

PET/CT acquisition

All scans were performed with a Siemens Inveon small-animal PET scanner (Siemens Healthcare, Knoxville, TN, USA). The mice used for the PET/CT examinations were fasted for 12–24 h, with access to water. The mice had their body weight measured, and they were anesthetized by isoflurane inhalation and injected via a tail-vein catheter with 10 MBq/0.1–0.2 mL of ^{18}F-FDG. The mice were then placed into the bed of the PET/CT scanner in the prone position, and a respiration pad was placed under their abdomen (Fig. 1a, b). The lung field was scanned with CT (field of view [FOV]: 32.0×32.0×48.1 mm^3) under 0.6 L/min air and 2% isoflurane inhalation. CT acquisition was performed while the waveform of breathing was measured, and a gating signal was acquired with a Biovet gating system (Biovet, M2Mimaging, Cleveland, OH, USA) with respiratory gating in the

inspiration phase. After CT acquisition, following a delay of 40-min to allow for FDG uptake, PET data were acquired for 20 min. We controlled the concentration of isoflurane under PET/CT imaging to stabilize the breathing of the mouse as much as possible. An example of a waveform is shown in Figure 1c.

Groups based on tumor volume

An analysis was performed based on the tumor size. The tumor volume was calculated based on the volume of interest (VOI) that was placed manually around the tumor on the CT image. We divided the mice into two groups. Small tumors were defined as those with a volume of less than 20 mm^3; large tumors were defined as those with a volume greater than 20 mm^3 (Table 1).

Non-gated (three-dimensional [3D]) and respiratory-gated (four-dimensional [4D]) histogramming and PET image reconstruction

List-mode data were sorted into a sinogram by use of three methods: (1) standard 3D PET sinograms (non-gated); (2) phase-based 4D PET sinograms with three gates (three bins); and (3) phase-based

4D PET sinograms with six gates (six bins) with use of the default span = 3, and maximum ring difference = 79. The scheme of a one-cycle breathing waveform under each gating method is shown in Fig. 2. With three bins, a one-cycle waveform was divided into an expiration phase (phase 1), a stable phase (phase 2), and an inspiration phase (phase 3). With six bins, each of the three phases above was divided into two (e.g., phase 2 was divided into phases 2-1 and 2-2). The sinogram files were reconstructed for 3 dimensions (3D) by use of one iteration of ordered-subject expectation maximization followed by 16 iterations of maximum a posteriori reconstruction (3D OS-EM/MAP [3D OS-EM (16 subsets), and MAP with a request resolution of 1.5mm]). Point spread functions (PSFs) were used in the projection matrix of the ordered subset expectation maximization in the 3D OS-EM/MAP algorithm. Neither an attenuation nor a scatter correction was applied.

Analysis of tumors

The PET images were analyzed by use of Inveon Research Workplace software. For all PET datasets, the VOI was defined manually in the transverse, sagittal, and coronal planes around the FDG uptake of the tumor, avoiding the FDG uptake of the heart. Using the region-grow algorithm, we thresholded the VOI at 40% of the maximum Bq/mL of the tumor (Fig. 3). A VOI was defined for

each phase of the gated PET dataset. We then automatically recorded the center coordinate of the VOI in the images involving six bins. The difference between the center coordinates in gated and non-gated PET images was used as the distance of respiratory movement.

We obtained values for the maximum standardized uptake values (SUV_{max}). For the gated study, the SUV_{max} was obtained for each phase. To compare the 3D and 4D SUV_{max}, we calculated the SUV_{max} percent difference between 3D and 4D PET. That is, % difference = [(4D PET SUV_{max} − 3D PET SUV_{max})/3D PET SUV_{max}] × 100 (%).

We correlated the % difference with tumor size. We examined the % difference in each phase and the average % difference over all phases. In addition, we selected the higher value for the % difference observed in phase 2-1 and phase 2-2, and designated the result as that from the "better bin".

Statistical analysis

The non-gated SUV_{max} and gated SUV_{max} were compared by use of the Wilcoxon signed-rank test (SPSS software, version 20, IBM Inc., New York, NY, USA). Phase-to-phase comparisons were made by use of Student's *t*-test. Throughout, *p* values smaller than 0.05 were assumed to indicate

statistical significance.

Results

Respiratory movement

The distance of respiratory movement for each phase is shown in Fig.4. In large tumors, the frequency of various respiratory-movement values was concentrated; the highest frequency occurred at 0.0 mm. However, among small tumors, the respiratory movement values were broadly dispersed.

SUV_{max} percent difference

PET images obtained under each condition are shown in Fig. 5. Tumor FDG uptake was higher in cases involving gated PET than in those involving non-gated PET, regardless of tumor size.

Tables 2-5 show the results for SUV_{max} and the % difference obtained for all conditions, and Fig. 6 shows the % difference in each phase. The 4D SUV_{max} were significantly higher than the 3D

SUV_{max}, regardless of the tumor size and the number of bins. The % difference was highest among small tumors in phase 2-1 (20.9 ± 9.7 %); however, there were no significant differences between the phases ($p > 0.06$). There was no significant difference in the % difference of large tumors between the phases, regardless of the number of bins.

Figures 7 and 8 show the correlation between the % difference and tumor volume in each condition; the correlation coefficients are shown in Table 6. With regard to six bins, there was a high correlation between the % difference in phase 2-2 and a small tumor volume ($r = 0.83$, $p = 0.01$); however, for three of the mice (Mice 4, 7, and 8), the % difference values were much lower than those for the other mice (Table 2). In cases involving a large tumor volume, no correlation was observed, regardless of the number of bins. The correlation between a value of the % difference observed in the "better bin" and tumor size was high in cases involving small tumors ($r = 0.83$, $p = 0.01$), but there was no correlation involving large tumors ($r = 0.10$, $p = 0.82$) (Fig. 8, Table 6). No correlation was observed in other conditions.

Discussion

Our study showed that the effect of respiratory movement was greater in cases involving small

tumors than in those involving large tumors. This finding was expected because the ratio of tumor volume to the distance of movement was larger for large tumors than that for small tumors. We assumed that tumors move a definitive distance over a definitive period of time. Therefore, the SUV_{max} observed under non-gated PET are considered to be more frequently underestimated in cases involving small tumors than in those involving large tumors. Consequently, the SUV_{max} % difference between gated and non-gated images for small tumors was larger than that for large tumors. These results are in agreement with those found in a phantom study (22).

In previous human PET studies, tumor FDG uptake values were determined for gated studies as the highest uptake ("best bin") in the respiratory period (12, 13). Vincente et al. (13) showed that most of the lesions (32/42 patients) had the highest SUV_{max} in the expiratory phase. Respiratory motion is low in the expiration phase, especially in the end-expiration phase (12, 15, 23), and good gated values may be obtained in such a low-respiratory-motion phase. In our study, the end-expiration phase was represented by the stable phase. Therefore, the best respiratory-gated imaging values were expected to be obtained in the stable phase. Consequently, in this study, we used three bins. However, there were no significant differences between the phases in cases involving three bins in either small or large tumors. These results suggest that respiratory gating with use of three bins is inadequate to correct for the effects of respiratory movement. In cases involving

six bins, the % difference was higher for the small tumors in the stable phase.

The best parameter for chronologically evaluating the FDG uptake of a tumor is controversial. Vincente et al. showed a correlation between tumor volume and % difference (13). Therefore, we looked for the quantitative value that showed the greatest correlation with tumor volume. In the case of six bins, we found that the % difference in the stable phase (phase2-2) had a high correlation with tumor volume. However, for three of the mice (Mice 4, 7, and 8), the % difference values were much lower than those for the other mice (Table 2). We considered that this difference is attributable to a difference in the respiratory state, that is, the respiratory rate as well as the respiratory depth. In the study, it was difficult to keep the respiratory state constant for all mice. Therefore, we suggest that consistent evaluation in one phase may be inappropriate, and we attempted to select the "better bin". The highest correlation between % difference and tumor volume was obtained when selecting the "better bin". Based on the results in our study and previous reports (12, 13), we consider respiratory gating with use of the stable phase and six bins to be the best method. Tumor FDG uptake values were quantified with use of higher SUV_{max} observed in the stable phase in cases involving small tumors.

In cases involving a large tumor volume, no correlation with % difference was observed in any of the cases. The large tumors evaluated in this study occupied approximately 30–60% of the lung

volume. A previous report showed that, if the lesion is large compared with the amplitude of motion, the effect on SUV_{max} will be small and 4D PET may not be necessary (23). This finding is consistent with the effects of respiratory movement in our study, where respiratory movement was small in cases involving large tumors. Therefore, a lack of correlation between the % difference and a large tumor volume may not be a problem. Consequently, it is not necessary to consider the degree of respiratory movement in cases involving large tumors. However, in chronologic studies evaluating the time course of tumor development, the same conditions may be used in mice with large tumors as those applied in mice with small tumors (i.e., performing gating in six bins and evaluating higher SUV_{max} in the stable phase). In chronologic studies of tumor development by PET, it is important to estimate the SUV_{max} rate of variability that accompanies the tumor volume rate of variability.

In PET/CT studies, CT images are used for attenuation correction and registration. We performed a gated CT scan in the deep inspiration phase; on the other hand, PET images were reconstructed in each respiratory phase. A CT-based attenuation correction was not applied because a mismatch of the tumor's location between PET and CT had been assumed. A mismatch of location between PET and CT can cause underestimation of SUV_{max} when CT data are used for attenuation correction (24-26). We showed that the most accurate SUV_{max} were obtained in the stable phase in PET images. We recommend that CT scans should be performed in the stable phase so that one can obtain highly

accurate quantitative results when using a CT-based attenuation correction. For mouse imaging, it is known that count recovery from attenuation correction is about 10-20 % with respect to the uncorrected images (27).

Conclusion

The most reliable SUV_{max} from respiratory-gated PET is obtained with the stable phase and six bins. The SUV_{max} observed with non-gated PET are underestimated more frequently in cases involving small tumors than in those involving large tumors. Therefore, researchers should be aware that the efficacy of respiratory-gated PET depends on tumor volume. In the chronologic study evaluating the time course of tumor development, the size of the tumor is small in early stage, and respiratory-gated PET is effective in reducing the underestimation of such tumors caused by respiratory motion.

Conflict of interest

The authors have no conflict of interest.

References

1. Poeppel TD, Krause BJ, Heusner TA, Boy C, Bockisch A, Antoch G. PET/CT for the staging and follow-up of patients with malignancies. Eur J Radiol. 2009;70(3):382–392.

2. Takeuchi S, Khiewvan B, Fox PS, Swisher SG, Rohren EM, Bassett RL Jr, et al. Impact of initial PET/CT staging in terms of clinical stage, management plan, and prognosis in 592 patients with non-small-cell lung cancer. Eur J Nucl Med Mol Imaging. 2013. doi: 10.1007/s00259-013-2672-8

3. Deroose CM, De Abhijit, Loening AM, Chow PL, Ray P, Chatziioannou AF, et al. Multimodality imaging of tumor xenografts and metastases in mice with combined small-animal PET, small-animal CT, and bioluminescence imaging. J Nucl Med. 2007;48:295-303.

4. Yamato M, Kataoka Y, Hiroshi M, Wada Y, Watanabe Y, et al. PET and macro- and microautoradiographic studies combined with immunohistochemistry for monitoring rat intestinal ulceration and healing processes. J Nucl Med. 2009;50:266-73.

5. P. E. Kinahan, D. W. Townsend, T. Beyer, and D. Sashin. Attenuation correction for a combined 3D PET/CT scanner. Med Phys. 1998;25: 2046-53

6. Timothy RD, Timothy GT, J. Jay Williams, Charles W. Stearns, John MH and R. Edward Coleman. Performance Characteristics of a Whole-Body PET Scanner. J

NucIMed1994;35:1398-1406

7. Goerres GW, Kamel E, Seifert B, Burger C, Buck A, Hany TF, et al. Accuracy of image coregistration of pulmonary lesions in patients with non-small cell lung cancer using an integrated PET/CT system. J Nucl Med. 2002;43:1469–75.

8. Mokhtar M, Kondo K, Takizawa H, Ohtani T, Otsuka H, Mitsuhiro, et al. Non-invasive monitoring of anticancer effects of cisplatin on lung cancer in an orthotopic SCID mouse model using [18F] FDG PET-CT. Oncology reports 2014;31:2007-2014.

9. Nehmeh SA, Erdi YE, Ling CC, Rosenzweig KE, Schoder H, Larson SM, et al. Effect of respiratory gating on quantifying PET images of lung cancer. J Nucl Med. 2002;43:876–81.

10. Nehmeh SA, Erdi YE, Pan T, Yorke E, Mageras GS, Rosenzweig KE, et al. Quantitation of respiratory motion during 4D-PET/CT acquisition. Med Phys. 2004;31:1333–8.

11. Dawood M, Büther F, Lang N, Schober O, Schaefers KP. Respiratory gating in positron emission tomography: a quantitative comparison of different gating schemes. Med Phys. 2007;34:3067–76.

12. Lupi A, Zaroccolo M, Salgarello M, Malfatti V, Zanco P. The effect of 18F-FDG-PET/CT respiratory gating on detected metabolic activity in lung lesions. Ann Nucl Med. 2009;23:191–6.

13. Garcia Vicente AM, Soriano Castreion A, Talavera Rubio MP, Leon Martin AA, Palomar Munoz AM, Pilkington Woll JP, et al. 18F-FDG PET-CT respiratory gating in characterization of pulmonary lesions: approximation towards clinical indications. Ann Nucl Med. 2010;24:207-14.

14. Elmpt Wv, Hamill J, Jodson J, Ruysscher DD, Lambin P, Michel Ollers L. Optimal gating compared to 3D and 4D PET reconstruction for characterization of lung tumors. Eur J Nucl Med Mol Imaging. 2011;38:843-55.

15. Kawano T, Ohtake E, Inoue T. Deep-inspiration breath-hold PET/CT versus free breathing PET/CT and respiratory gating PET for reference: evaluation in 95 patients with lung cancer. Ann Nucl Med. 2011;25:109-16.

16. Kim SC, Machac J, Krynyckyi BR, Knesaurek K, Krellenstein D, Schultz B, et al. FDG PET for evaluation of indeterminate lung nodules: assigning a probability of malignancy may be preferable to binary readings. Ann Nucl Med. 2008;22:165–70.

17. Kesner AL, Abourben G, Mishani E, Chisin R, Tshori Sagi, Freedman N. Gating, enhanced gating, and beyond: information utilization strategies for motion management, applied to preclinical PET. Eur J Nucl Med Mol Imaging. 2013;3(29).

18. Ishikura H, Kondo K, Miyoshi T et al. Artificial Lymphogenous Metastatic Model Using

Orthotopic Implantation of Human Lung Cancer. Ann Thorac Surg 2000; 69:1691-5.

19. Fujino H, Kondo K, Ishikura H et al. Matrix metalloproteinase inhibitor MMI-166 inhibits lymphogenous metastasis in an orthotopically implanted model of lung cancer. Mol Cancer Ther 2005;4:1409-16.

20. Toyama H, Ichise M, Liow J-S, et al. Evaluation of anesthesia effects on [18F]FDG uptake in mouse brain and heart using small animal PET. J Nucl Med. 2004;(31):251-56

21. Judith E.F, Leanne M.M, Alexander V et al. The Effects of Anesthetic Agent and Carrier Gas on Blood Glucose and Tissue Uptake in Mice Undergoing Dynamic FDG-PET Imaging: Sevoflurane and Isoflurane Compared in Air and in Oxygen. Mol Imaging Bid. 2008;(10):192-200

22. Pevsner A, Nehmeh SA, Humm JL, Mageras GS, Erdi YE. Effect of motion on tracer activity determination in CT attenuation corrected PET images: A lung phantom study. Med. Phys. 2005;32(7):2358-62

23. Teo BK, Saboury B, Munbodh R, Scheuermann J, Torigian DA, Zaidi H, et al. The effect of breathing irregularities on quantitative accuracy of respiratory gated PET/CT. Med. Phys. 2012;39(12):7390-7

24. Rosario T, Ollers MC, Bosmans G, Ruysscher DD, Lambin P, Dekker A. Phased versus

midventilation attenuation-corrected respiration-correlated PET for patients with non–small cell lung cancer. J Nucl Med. 2009;37:208-14.

25. Nagel CC, Bosmans G, Dekker AL, Ollers MC, De Ruysscher DK, Lambin P, et al. Phased attenuation correction in respiration correlated computed tomography/positron emitted tomography. Med Phys. 2006;33:1840–7.

26. Callahan J, Kron T, Schneider-K M, J. Hicks R. The clinical significance and management of lesion motion due to respiration during PET/CT scanning. Cancer Imaging. 2011;11;224-36

27. D'Ambrosio D, Zagni F, Spinelli AE., Marengo M. Attenuation correction for small animal PET images: a comparison of two methods. Computational and Mathematical Methods in Medicine. 2013 (2013), Article ID 103476, 12 pages

Figure legends

Fig. 1 (a) Respiration sensor pad. (b) Positioning of the mice and placement of the respiratory sensor pads. (c) Example of a waveform during breathing.

Fig. 2 Scheme of a one-cycle waveform during breathing in a mouse, and the method used for dividing the waveform on gated PET.

Fig. 3 (a) CT axial view. (b) PET axial view in the same slice with a CT image (Fig.3 (a)) and defined VOI on the tumor. The Outside VOI was defined manually, the inside one was thresholded at 40%. The center coordinates of the VOI were automatically represented; the center coordinate of the VOI in this figure was (x (sagittal), y (coronal), z (transverse)) = (-6.3, -0.4, 0.8).

Fig. 4 Plotted differences between the center coordinates of the VOI on gated PET in each phase and non-gated PET in each axis. (a) Horizontal axis = X axis, longitudinal axis = Y axis; (b) horizontal axis = X axis, longitudinal axis = Z axis; (c) horizontal axis = Y axis, longitudinal axis = Z axis. (d) Histogram of the differences in all axes.

Fig. 5 PET images under each condition (small tumor, mouse 1; large tumor, mouse 16). The value in the top right of the image shows the SUV_{max} of the tumor.

Fig. 6 Percent difference in each phase in the cases involving six bins (left) and in the cases involving three bins (right).

Fig. 7 Analysis of the correlations between the % difference in each phase and tumor volume in the cases involving six bins (a), and in cases involving three bins (b). Triangles indicate the average % difference for each phase and the curve-fitting line.

Fig. 8 Analysis of the correlations between the higher values of % difference in the stable phase (phase 2-1 and phase 2-2) and tumor volume in the cases involving six bins. White circles indicate the % difference in cases involving small tumors, and black circles indicate the % difference in cases involving large tumors.

Fig. 1 (a) Respiration sensor pad. (b) Positioning of the mice and placement of the respiratory sensor pads. (c) Example of a waveform during breathing.

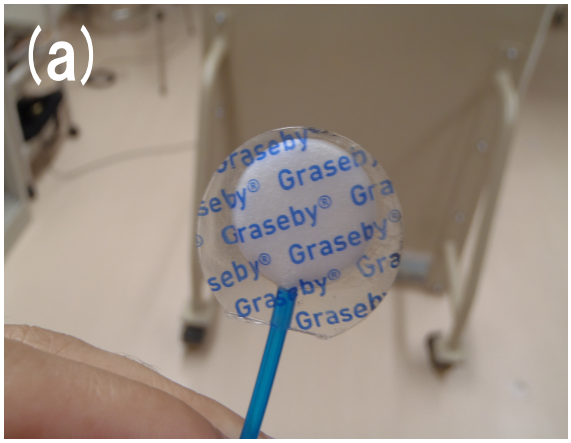

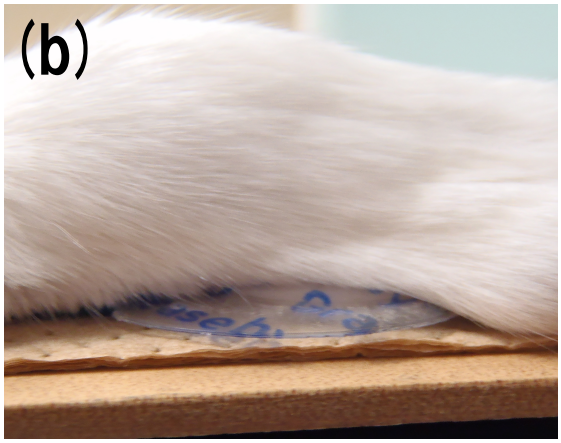

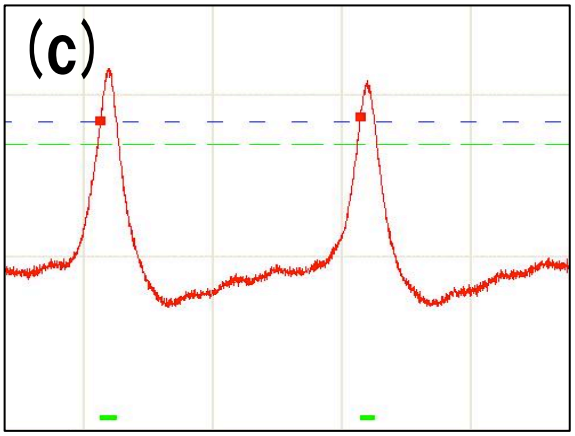

Fig. 2 Scheme of a one-cycle waveform during breathing in a mouse, and the method used for dividing the waveform on gated PET.

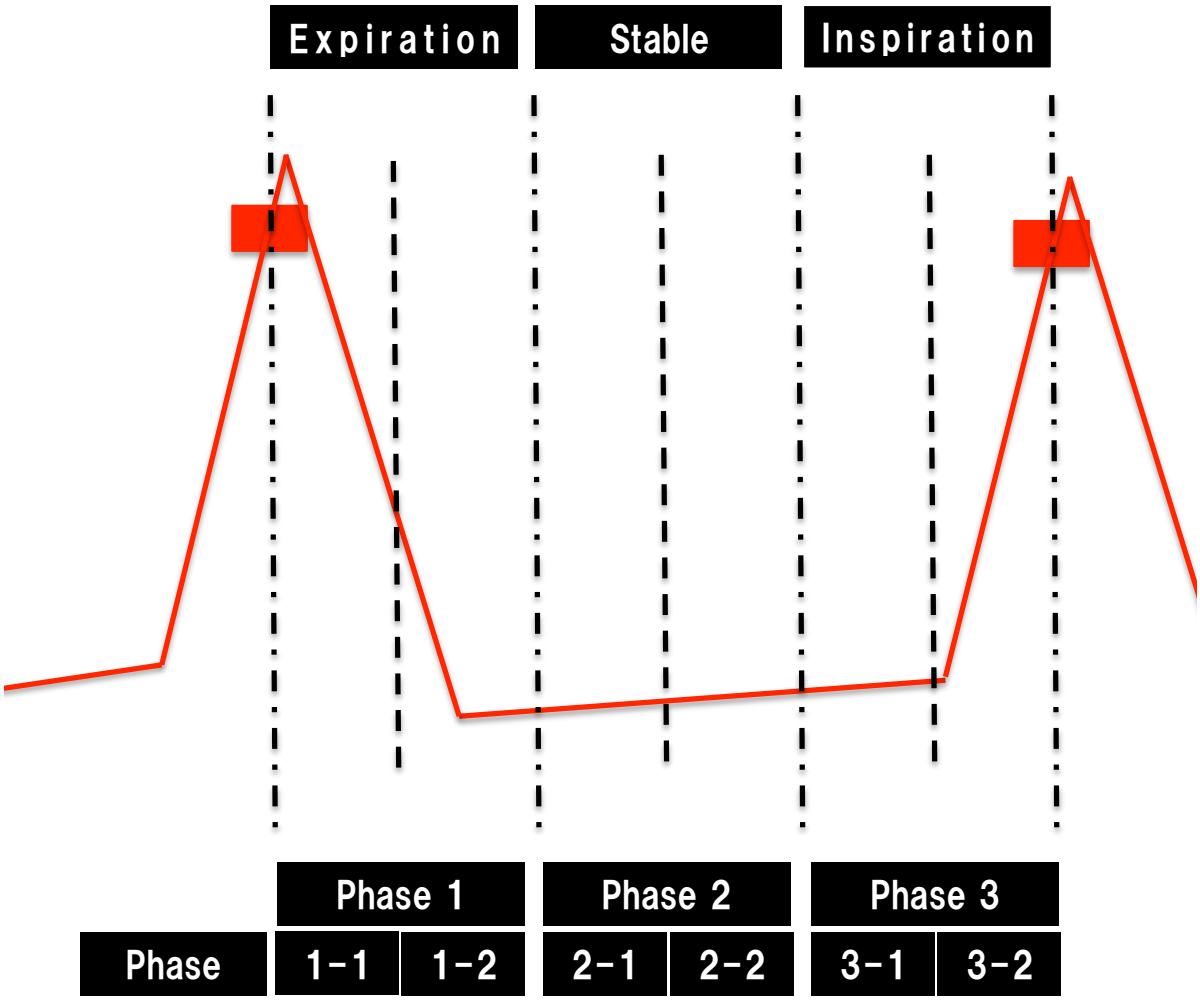

Fig. 3 (a) CT axial view. (b) PET axial view in the same slice with a CT image (Fig.3 (a)) and defined VOI on the tumor. The Outside VOI was defined manually, the inside one was thresholded at 40%. The center coordinates of the VOI were automatically represented; the center coordinate of the VOI in this figure was (x (sagittal), y (coronal), z (transverse)) = (-6.3, -0.4, 0.8).

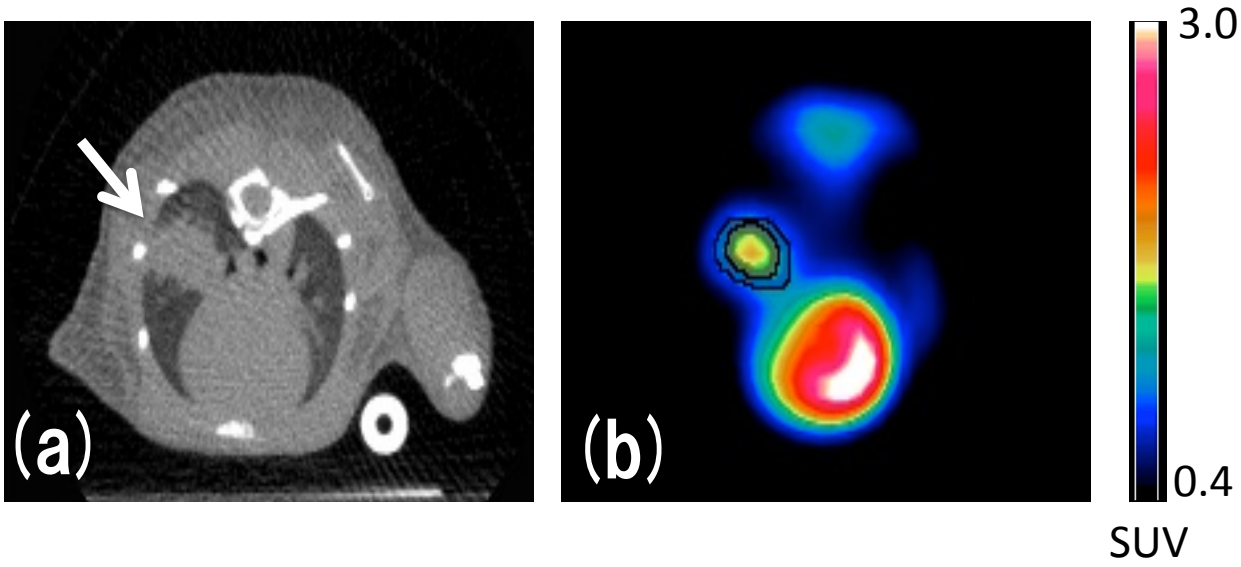

Fig. 4 Plotted differences between the center coordinates of the VOI on gated PET in each phase and non-gated PET in each axis. (a) Horizontal axis = X axis, longitudinal axis = Y axis; (b) horizontal axis = X axis, longitudinal axis = Z axis; (c) horizontal axis = Y axis, longitudinal axis = Z axis. (d) Histogram of the differences in all axes.

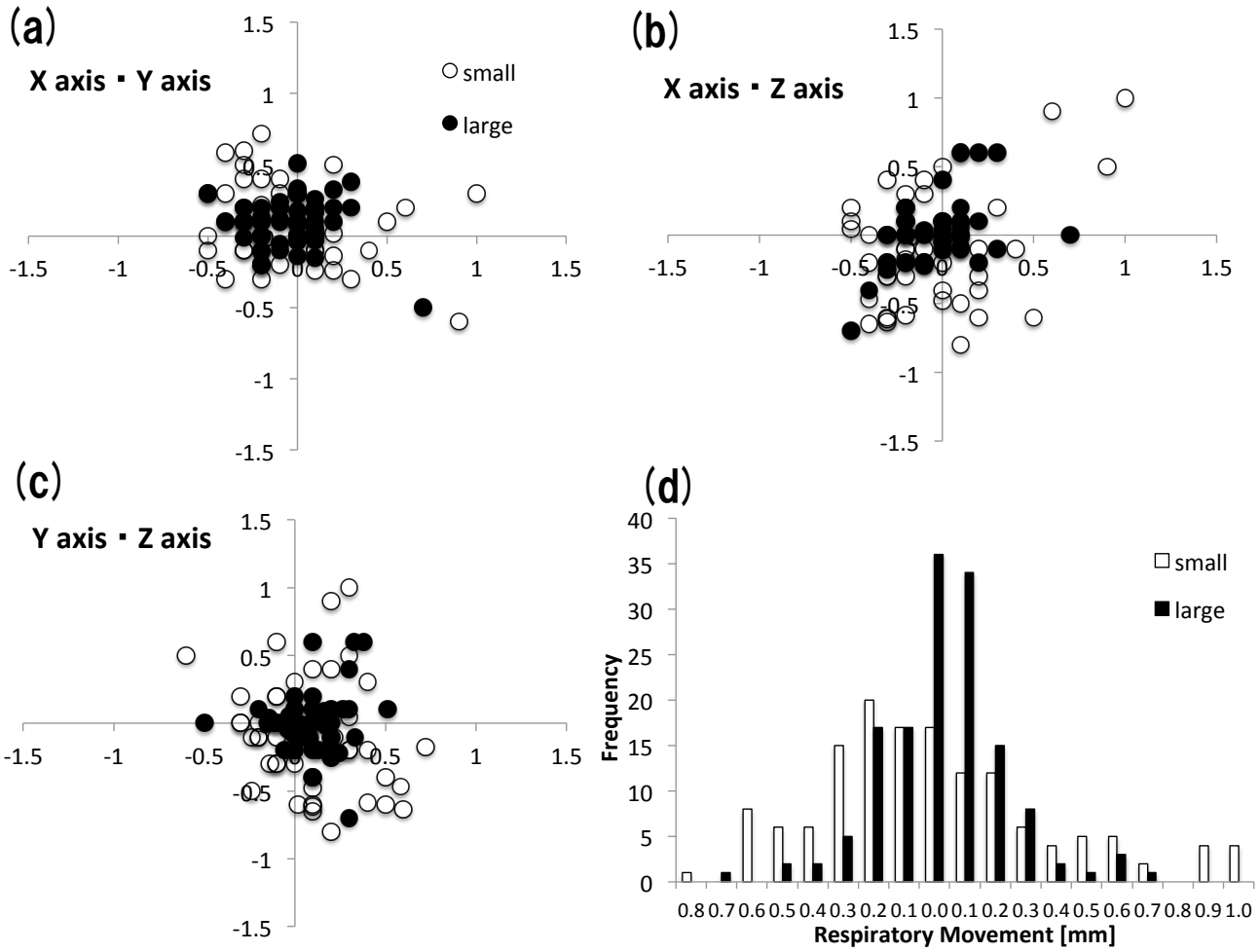

Fig. 5 PET images under each condition (small tumor, mouse 5; large tumor, mouse 10). The value in the top right of the image shows the SUV_{max} of the tumor.

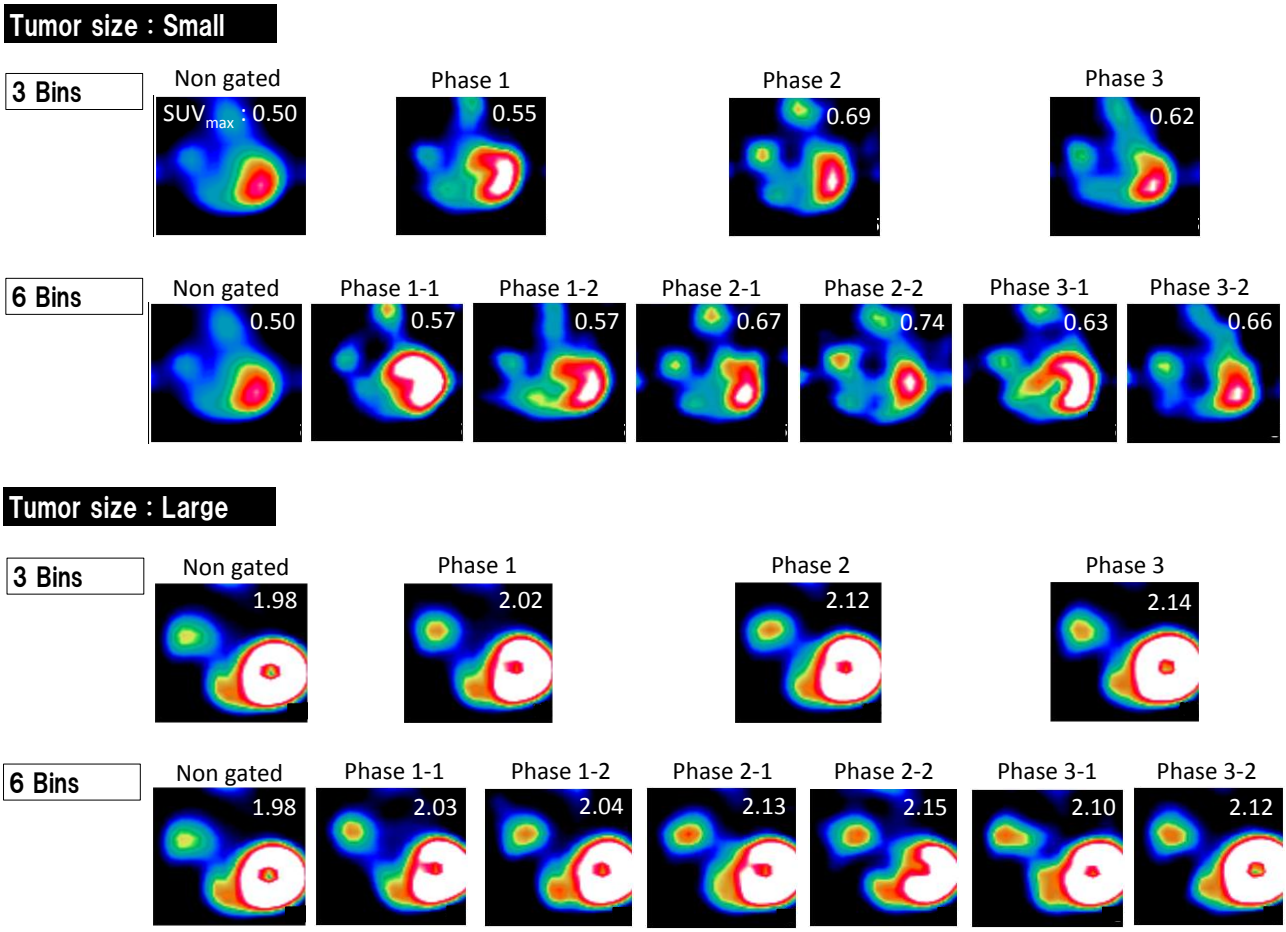

Fig. 6 Percent difference in each phase in the cases involving six bins (left) and in the cases involving three bins (right).

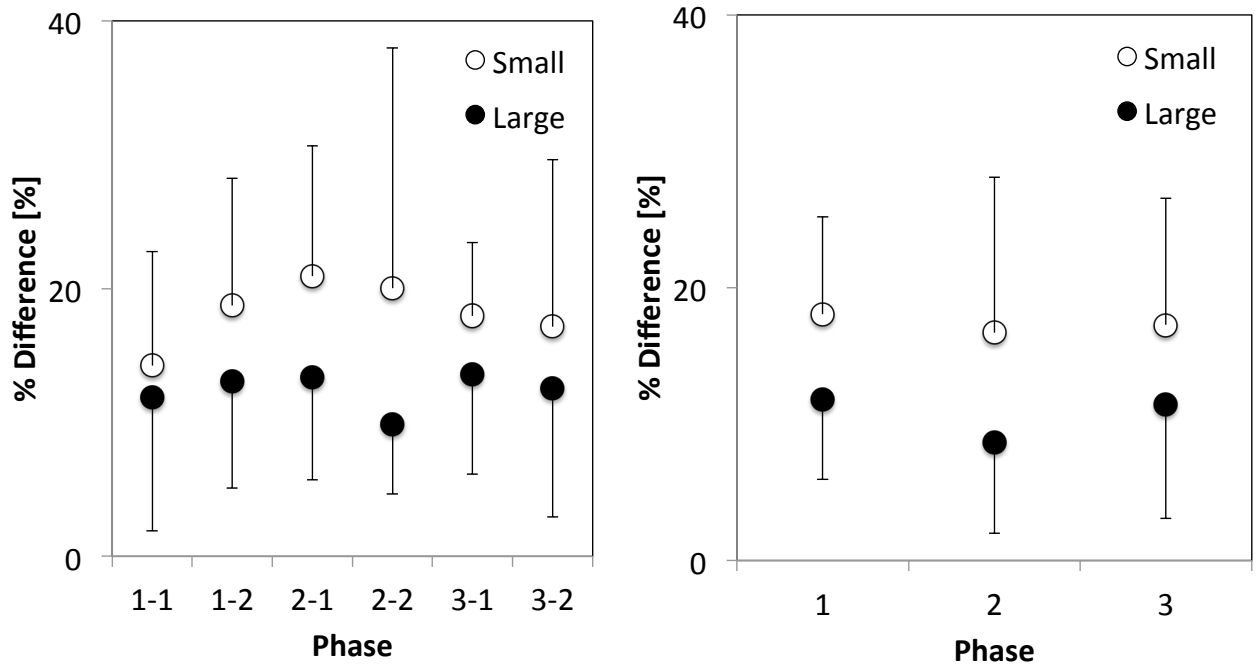

Fig. 7 Analysis of the correlations between the % difference in each phase and tumor volume in the cases involving six bins (a), and in cases involving three bins (b). Triangles indicate the average % difference for each phase and the curve-fitting line.

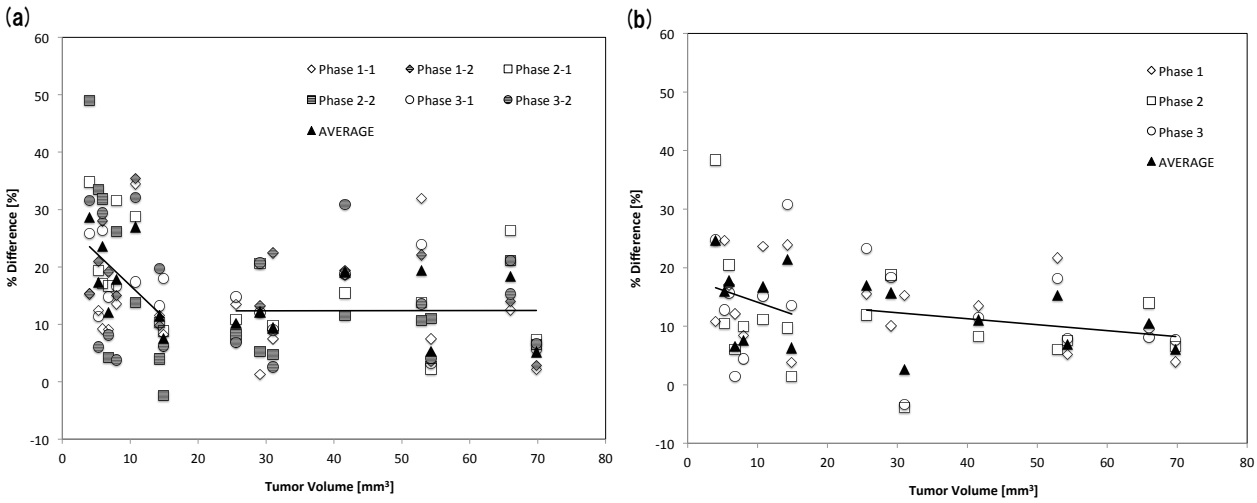

Fig. 8 Analysis of the correlations between the higher values of % difference in the stable phase (phase 2-1 and phase 2-2) and tumor volume in the cases involving six bins. White circles indicate the % difference in cases involving small tumors, and black circles indicate the % difference in cases involving large tumors.

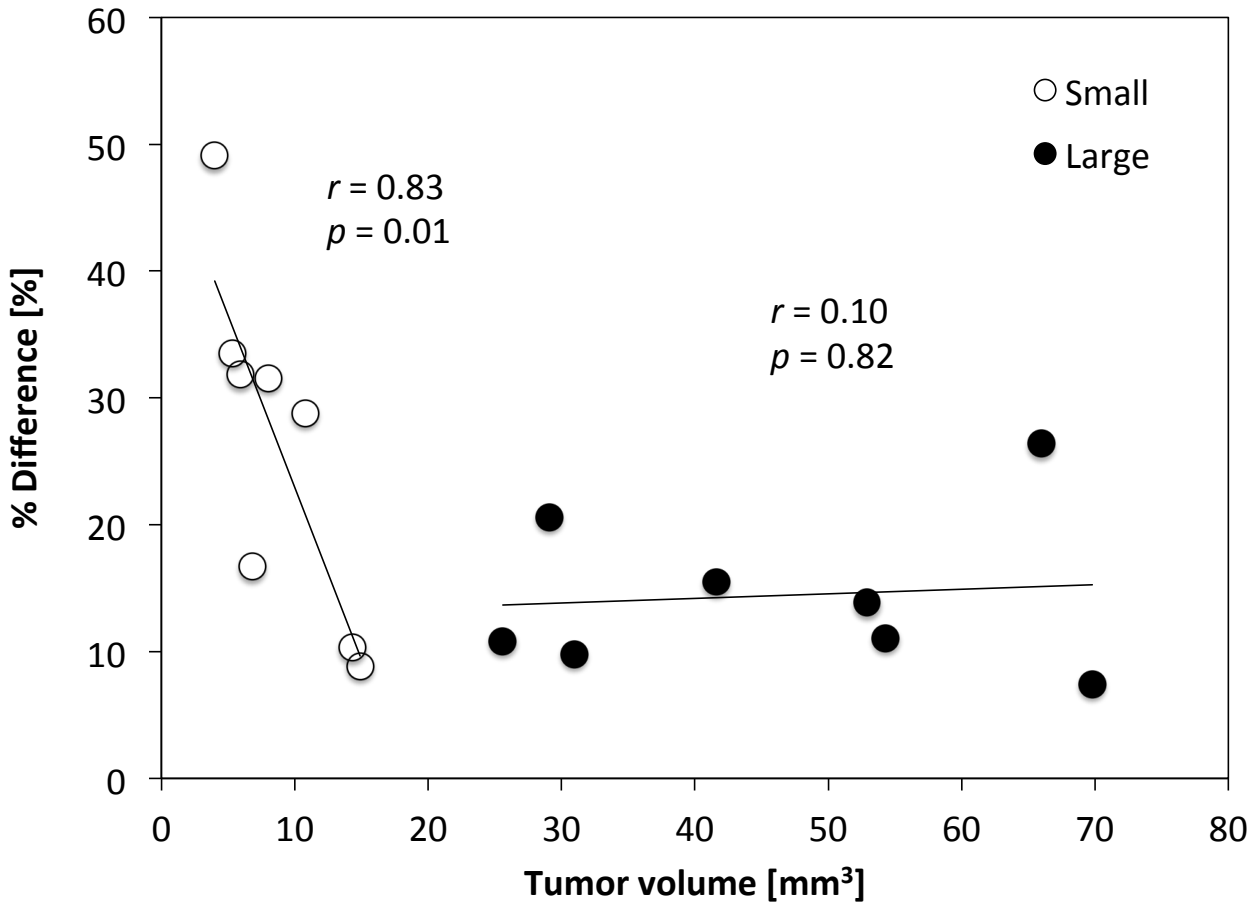

Table 1. Characteristics of the mice and tumors (cell lines, days after transplantation of the tumor, and tumor volume). There were eight mice in each group.

		Cell lines	Days	Tumor Volume [mm^3]
Small	Mouse 1	A549	28	4.0
	Mouse 2	Ma44-3	6	5.3
	Mouse 3	A549	22	5.9
	Mouse 4	A549	33	6.8
	Mouse 5	Ma44-3	8	8.0
	Mouse 6	A549	33	10.8
	Mouse 7	Ma44-3	8	14.3
	Mouse 8	A549	33	14.9
	Mean ± SD			8.7 ± 4.1
Large	Mouse 9	Ma44-3	13	25.6
	Mouse 10	A549	45	29.1
	Mouse 11	A549	45	31.0
	Mouse 12	A549	40	41.6
	Mouse 13	A549	52	52.9
	Mouse 14	A549	49	54.3
	Mouse 15	Ma44-3	13	66.0
	Mouse 16	Ma44-3	13	69.8
	Mean ± SD			46.3 ± 17.0

Table 2 Characteristics of mice and small tumors (SUVmax and % difference in each phase) in cases involving six bins.

		Non gated	Phase 1-1	Phase 1-2	Phase2-1	Phase 2-2	Phase 3-1	Phase 3-2	Mean (gated) ± SD
Mouse1	SUVmax	0.50	0.57	0.57	0.67	0.74	0.63	0.65	0.64 ± 0.06
	% Difference		14.00	14.00	34.00	48.00	26.00	30.00	27.67 ± 12.93
Mouse2	SUVmax	0.48	0.54	0.58	0.58	0.64	0.54	0.51	0.57 ± 0.05
	% Difference		12.50	20.83	20.83	33.33	12.50	6.25	17.71 ± 9.48
Mouse3	SUVmax	0.50	0.54	0.64	0.58	0.66	0.63	0.64	0.62 ± 0.05
	% Difference		8.00	28.00	16.00	32.00	26.00	28.00	23.00 ± 9.10
Mouse4	SUVmax	0.69	0.75	0.82	0.80	0.72	0.79	0.75	0.77 ± 0.04
	% Difference		8.70	18.84	15.94	4.35	14.49	8.70	11.98 ± 5.46
Mouse5	SUVmax	0.72	0.82	0.83	0.95	0.91	0.85	0.75	0.85 ± 0.07
	% Difference		13.89	15.28	31.94	26.39	18.06	4.17	17.55 ± 9.74
Mouse6	SUVmax	0.74	1.00	1.01	0.96	0.85	0.87	0.98	0.95 ± 0.07
	% Difference		35.14	36.49	29.73	14.86	17.57	32.43	27.01 ± 9.19
Mouse7	SUVmax	0.72	0.80	0.79	0.79	0.74	0.81	0.86	0.80 ± 0.04
	% Difference		11.11	9.72	9.72	2.78	12.50	19.44	11.50 ± 5.40
Mouse8	SUVmax	0.87	0.94	0.92	0.95	0.85	1.02	0.92	0.93 ± 0.06
	% Difference		8.05	5.75	9.20	-2.30	17.24	5.75	7.44 ± 6.33
Average	SUVmax	0.65 ± 0.14	0.75 ± 0.18	0.77 ± 0.16	0.79 ± 0.16	0.76 ± 0.10	0.77 ± 0.16	0.76 ± 0.16	
	% Difference		13.92 ± 8.92	18.61 ± 9.93	20.92 ± 9.87	19.93 ± 17.77	18.05 ± 5.37	16.84 ± 12.01	
	p value (vs. 3D)		0.012	0.012	0.012	0.017	0.012	0.012	

Table 3 Characteristics of mice and large tumors (SUVmax and % difference in each phase) in cases involving six bins.

		Non gated	Phase 1-1	Phase 1-2	Phase2-1	Phase 2-2	Phase 3-1	Phase 3-2	Mean (gated) ± SD
Mouse9	SUVmax	1.43	1.62	1.53	1.59	1.55	1.64	1.53	1.58 ± 0.04
	% Difference		13.29	6.99	11.19	8.39	14.69	6.99	10.26 ± 3.02
Mouse10	SUVmax	0.97	0.98	1.10	1.17	1.02	1.09	1.17	1.09 ± 0.07
	% Difference		1.03	13.40	20.62	5.15	12.37	20.62	12.20 ± 7.28
Mouse11	SUVmax	0.90	0.97	1.10	0.99	0.94	0.98	0.92	0.98 ± 0.06
	% Difference		7.78	22.22	10.00	4.44	8.89	2.22	9.26 ± 6.37
Mouse12	SUVmax	0.95	1.13	1.14	1.10	1.06	1.13	1.25	1.14 ± 0.06
	% Difference		18.95	20.00	15.79	11.58	18.95	31.58	19.48 ± 6.10
Mouse13	SUVmax	0.92	1.21	1.12	1.04	1.01	1.13	1.04	1.09 ± 0.07
	% Difference		31.52	21.74	13.04	9.78	22.83	13.04	18.66 ± 7.46
Mouse14	SUVmax	1.16	1.25	1.20	1.19	1.29	1.20	1.21	1.22 ± 0.04
	% Difference		7.76	3.45	2.59	11.21	3.45	4.31	5.46 ± 3.05
Mouse15	SUVmax	1.52	1.71	1.73	1.92	1.84	1.84	1.75	1.80 ± 0.07
	% Difference		12.50	13.82	26.32	21.05	21.05	15.13	18.31 ± 4.89
Mouse16	SUVmax	1.98	2.03	2.04	2.13	2.12	2.10	2.12	2.09 ± 0.04
	% Difference		2.53	3.03	7.58	7.07	6.06	7.07	5.56 ± 2.02
Average	SUVmax	1.23 ± 0.39	1.36 ± 0.38	1.37 ± 0.36	1.39 ± 0.43	1.35 ± 0.44	1.39 ± 0.41	1.37 ± 0.40	
	% Difference		11.92 ± 9.83	13.08 ± 7.91	13.39 ± 7.48	9.83 ± 5.23	13.54 ± 7.11	12.40 ± 5.78	
	p value (vs. 3D)		0.012	0.012	0.012	0.012	0.012	0.012	

Table 4 Characteristics of mice and small tumors (SUVmax and % difference in each phase) in cases involving three bins.

		Non gated	Phase 1	Phase 2	Phase 3	Mean (gated) ± SD
Mouse1	SUVmax	0.50	0.55	0.69	0.62	0.62 ± 0.07
	% Difference		10.00	38.00	24.00	24.00 ± 14.00
Mouse2	SUVmax	0.48	0.60	0.53	0.54	0.56 ± 0.04
	% Difference		25.00	10.42	12.50	15.97 ± 7.89
Mouse3	SUVmax	0.50	0.58	0.60	0.58	0.59 ± 0.01
	% Difference		16.00	20.00	16.00	17.33 ± 2.31
Mouse4	SUVmax	0.69	0.77	0.73	0.70	0.73 ± 0.04
	% Difference		11.59	5.80	1.45	6.28 ± 5.09
Mouse5	SUVmax	0.72	0.79	0.80	0.76	0.78 ± 0.02
	% Difference		9.72	11.11	5.56	8.80 ± 2.89
Mouse6	SUVmax	0.74	0.92	0.83	0.86	0.87 ± 0.05
	% Difference		24.32	12.16	16.22	17.57 ± 6.19
Mouse7	SUVmax	0.72	0.89	0.79	0.94	0.87 ± 0.08
	% Difference		23.61	9.72	30.56	21.30 ± 10.61
Mouse8	SUVmax	0.87	0.90	0.88	0.99	0.92 ± 0.06
	% Difference		3.45	1.15	13.79	6.13 ± 6.73
Average	SUVmax	0.65 ± 0.14	0.75 ± 0.15	0.73 ± 0.12	0.75 ± 0.17	
	% Difference		15.46 ± 8.09	13.55 ± 11.25	15.01 ± 9.30	
	p value (vs. 3D)		0.012	0.012	0.012	

Table 5 Characteristics of mice and large tumors (SUVmax and % difference in each phase) in cases involving three bins.

		Non gated	Phase 1	Phase 2	Phase 3	Mean (gated) ± SD
Mouse9	SUVmax	1.43	1.65	1.60	1.76	1.67 ± 0.07
	% Difference		15.38	11.89	23.08	16.78 ± 4.67
Mouse10	SUVmax	0.97	1.07	1.15	1.15	1.12 ± 0.04
	% Difference		10.31	18.56	18.56	15.81 ± 3.89
Mouse11	SUVmax	0.90	1.04	0.86	0.87	0.92 ± 0.08
	% Difference		15.56	-4.44	-3.33	2.60 ± 9.18
Mouse12	SUVmax	0.95	1.08	1.03	1.06	1.06 ± 0.02
	% Difference		13.68	8.42	11.58	11.23 ± 2.16
Mouse13	SUVmax	0.92	1.11	0.97	1.08	1.05 ± 0.06
	% Difference		20.65	5.43	17.39	14.49 ± 6.54
Mouse14	SUVmax	1.16	1.22	1.25	1.25	1.24 ± 0.01
	% Difference		5.17	7.76	7.76	6.90 ± 1.22
Mouse15	SUVmax	1.52	1.66	1.73	1.64	1.68 ± 0.04
	% Difference		9.21	13.82	7.89	10.31 ± 2.54
Mouse16	SUVmax	1.98	2.06	2.12	2.14	2.11 ± 0.03
	% Difference		4.04	7.07	8.08	6.40 ± 1.72
Average	SUVmax	1.23 ± 0.39	1.36 ± 0.38	1.34 ± 0.44	1.37 ± 0.43	
	% Difference		11.75 ± 5.63	8.56 ± 6.77	11.38 ± 8.26	
	p value (vs. 3D)		0.012	0.017	0.017	

Table 6 Correlation coefficients for all conditions.

		Correlation coefficients	
		Small (p value)	Large (p value)
6 Bins	Phase 1-1	0.06 (0.88)	0.06 (0.90)
	Phase 1-2	0.40 (0.33)	0.30 (0.47)
	Phase 2-1	0.59 (0.12)	3.46×10^{-3} (0.99)
	Phase 2-2	0.83 (0.01)	0.55 (0.16)
	Phase 3-1	0.37 (0.36)	8.49×10^{-3} (0.98)
	Phase 3-2	0.17 (0.70)	0.09 (0.84)
	AVERAGE	0.60 (0.11)	4.36×10^{-3} (0.99)
3 Bins	Phase 1	0.05 (0.91)	0.47 (0.24)
	Phase 2	0.64 (0.09)	0.02 (0.96)
	Phase 3	0.26 (0.53)	0.28 (0.51)
	AVERAGE	0.24 (0.56)	0.34 (0.42)
6 Bins	Better bin in Stable phase	0.83 (0.01)	0.10 (0.82)